

Accepted for publication: August 11, 2017

Publisher version: Warfvinge, K., KleinHeerenbrink, M. & Hedenström, A. 2017 The power–speed relationship is U-shaped in two free-flying hawkmoths (*Manduca sexta*). J. R. Soc. Interface 14, 20170372. (doi:10.1098/rsif.2017.0372)

The Power-Speed Relationship is U-Shaped in Two Free-Flying Hawkmoths (*M. sexta*)

Kajsa Warfvinge¹, Marco KleinHeerenbrink², Anders Hedenström¹

Affiliations: ¹ Department of Biology, Lund University, Lund, Sweden; ² Department of Zoology, University of Oxford, Oxford, UK

Author for correspondence: Kajsa Warfvinge, email: Kajsa.Warfvinge@biol.lu.se

Keywords: insect, hawkmoth, power, aerodynamics, tomographic particle image velocimetry

Abstract

A flying animal can minimise its energy consumption by choosing an optimal flight speed depending on the task at hand. Choice of flight speed can be predicted by modelling the aerodynamic power required for flight, and this tool has previously been used extensively in bird migration research. For insects, however, it is uncertain whether any of the commonly used power models are useful, as insects often operate in a very different flow regime from vertebrates. To investigate this, we measured aerodynamic power in the wake of two *Manduca sexta* flying freely in a wind tunnel at 1–3.8 ms⁻¹, using tomographic particle image velocimetry (tomo-PIV). The expended power was similar in magnitude to that predicted by two classic models. However, the most ubiquitously used model, originally intended for vertebrates, failed to predict the sharp increase in power at higher speeds, leading to an overestimate of predicted flight speed during longer flights. In addition to measuring aerodynamic power, the tomo-PIV system yielded a highly detailed visualisation of the wake, which proved to be significantly more intricate than could be inferred from previous smoke trail- and 2D-PIV studies.

1 Introduction

Flight is an energetically demanding method of locomotion. It is therefore natural to assume that there is a selective pressure to economise power usage during flight. There can be multiple optimisation objectives, depending on the task at hand: Maximising flight duration on a given energy budget is the aim when *e.g.* performing display flight [1]. In migration, or other longer flights, it may be more beneficial to minimise the power per distance travelled [2]. If it is of essence to arrive to the breeding grounds early to acquire a territory, time spent on migration is a reasonable currency to minimise. In all these examples, the optimisation strategy leads to a choice of flight speed, which can be predicted based on how the power required to fly scales with flight speed. In the order mentioned, these are the minimum power speed (u_{mp}), maximum range speed (u_{mr}) and the optimal speed to minimise time of migration (u_{mt}).

In vertebrates, the flight speed–power relationship is often modelled as a U-shaped curve, defined by a number of morphological and kinematic parameters. The model was first adapted to bird flight from aeroplane theory by Pennycuik [2, 3], and its simplicity has allowed it to be ubiquitously used to, among other things, predict flight behaviour in migrating birds [4]. The flight speed–power relationship predicted from the model has, for bird flight, been qualitatively supported by empirical data [5, 6]. Some behaviours, such as responses to different wind conditions, can be predicted by qualitative aspects of the model alone (the U-shape). A testable example of this is the prediction that individuals choosing to fly at u_{mr} should increase their speed in headwinds and decrease it in tailwinds, while behaving unaffected by wind when selecting u_{mp} [4].

Although Pennycuick's model was originally created for vertebrates, the theory behind a U-shaped power curve is in fact very general, and could, in principle, be applied also to other taxa, such as insects. Female (but not male) *Phoebis sennae* migrating over the Caribbean Sea have shown behaviour consistent with a U-shaped curve: the butterflies decreased their speed in tailwinds [7]. However, measurements on flight power have qualitatively been in disagreement with such a model. As an example, metabolic measurements on bumblebees [8] describe a flat, almost horizontal relationship between power and speed. Additionally, a number of computational fluid dynamics (CFD) studies have suggested that the power curve in insects may be J-shaped, so that the power during hover is comparable to the minimum power (fruit fly: [9]; bumblebee: [10]). There are many reasons for why a simple model developed for vertebrate flight should not be suitable for insects, especially considering that flight at these small scales relies heavily on unsteady aerodynamics, which the model ignores [2]. An obvious example of such an effect is the leading edge vortex, which has been shown to contribute significantly to lift force in hawkmoths (*Manduca sexta*: [11]; *Macroglossum stellatarum*: [12]).

While not directly incorporating unsteady aerodynamics, several authors have modelled insect flight with more realistic wing kinematics than does Pennycuick's model, for example using a blade-element approach [13, 14, 15]. The method divides the wing into strips with computations done separately for each element; in some cases averaging coefficients over the down- and upstroke. The result is in most cases an aerodynamic power that is similar in magnitude to that predicted by Pennycuick's model, but with different derived characteristic flight speeds. None of these models have, however, been empirically validated.

The hawkmoth *Manduca sexta* is one of the species for which attempts at predicting aerodynamic power have previously been made [15]. *M. sexta* has long been a model species for studies in both sensory biology and flight mechanics due to its large size, stable flight and the ability to be trained to fly in place at a feeder. Both this and other hawkmoths have also been the focus of CFD (computational fluid dynamics) studies. Together, this makes *M. sexta* an ideal candidate for evaluation of the power models. The wake generated by hawkmoths is to some extent unknown, but has previously been studied in tethered individuals with techniques of flow visualisation using smoke trails [16] and 2-dimensional particle image velocimetry (PIV) recording approximately one frame per wingbeat [17].

Our aims with this study were twofold: First, we wanted to investigate whether previous interpretations of the wake structure of *M. sexta* are reasonable. A wake is the flying animal's aerodynamic "footprint", and as such carries information about how flight forces were produced. Visualising the wake can therefore help to clarify the aerodynamic functions of the up- and downstroke as well as the different parts of the wings and body. We produced detailed reconstructions of the hawkmoth wake using a time-resolved three-dimensional flow visualisation system (tomographic particle image velocimetry, or tomo-PIV). The moths were flying freely in a wind tunnel at air speeds between 1 and 3.8 ms⁻¹, and the range of speeds investigated allowed for a second aim: We adapted a method (based on [18]) for directly measuring the aerodynamic power, enabling us to evaluate whether any of the aforementioned simplified models can be used to accurately predict power output of insect flight, and hence serve as a tool to predict flight behaviour. The fact that a tomo-PIV system was used allowed us to acquire volumes of 3-dimensional velocity fields, from which we calculated the aerodynamic power as the rate of energy added to the air by the animal. While a similar computational method has been used with stereo-PIV data in [19], the fact that we were able to measure 3-dimensional velocity gradients allowed us to calculate aerodynamic power with greater accuracy.

Methods

Study Species and Training

Four newly eclosed *Manduca sexta* were acquired from the Swedish University of Agricultural Sciences in Alnarp, Sweden. After a few days of starvation, each moth was moved to the low turbulence Lund

Table 1. Morphological and kinematic data for the two *M. sexta* used in this study.

Parameter	Unit	M1	M2
Body mass (m)	g	2.3	1.8
Wing span (b)	m	0.119	0.104
Wing area (S)	m ²	0.0026	0.0020
Frontal body area (S_b)	m ²	0.00018	0.00018
Aspect ratio (AR)	–	5.5	5.5
Reynolds number (Re)	–	1500–5800	1300–5000
Wingbeat frequency (f)	s ⁻¹	26.6	28.6

University wind tunnel (described in [20]), where experiments were immediately started. In the center of the test section an artificial blue flower was placed, which provided the moths with a 15% honey solution, scented with lavender oil. This allowed us to control the moths' flight position in the wind tunnel. All experiments were conducted in dim light, comparable to conditions at dusk. Air speed in the wind tunnel was set to 1, 2, 2.8–2.9 and 3.8 ms⁻¹, as we wanted to investigate speeds both lower and higher than the preferred speed of the species (3 ms⁻¹; [21]). At 3.8 ms⁻¹ the animals had obvious difficulties flying stably at the feeder; hence no measurements at higher speeds were possible.

Two of the moths were eliminated from the dataset, as they did not generate data for all flight speeds in the range. During experiments, one individual damaged its wings to such a degree that it could not complete flight at all speeds. The wakes of a second individual were not completely captured at 1 and 3.8 ms⁻¹, due to a suboptimal vertical placement of the moth. The dataset hence consists of data from two moths, M1 and M2.

Experimental Setup

Tomographic PIV

To visualise the wake vortices and from them measure flight forces and power output, we used a tomographic PIV system (LaVision GmbH) consisting of a 527 nm Nd-YLF double-cavity laser (Litron Lasers Ltd, model LDY304PIV) and four high-speed cameras (Imager Pro HS 4, 2016 × 2016 pixels) (Figure 1). The system was seeded with a mist of Di-Ethyl-Hexyl-Sebacat smoke fluid and run at 640 Hz repetition rate. A 14 mm thick illuminated volume was produced by letting the relatively focused laser beam bounce between two 100 × 100 mm² mirrors to build up the height of the volume. PIV analysis was done in LaVision DaVis 8.15 by pre-processing (subtract sliding minimum, normalise with local average, Gaussian smoothing and sharpening), reconstructing the particles in 3D space (fast MART algorithm, four iterations, resulting in approximately 220 × 3000 × 1800 voxels), correlating the two reconstructed volumes (window size stepwise decreasing from 96 × 96 × 96 to 48 × 48 × 48 voxels with 75% overlap) and vector post processing (3 × 3 × 3 smoothing). The resulting vector fields consisted of approximately 18 × 220 × 125 vectors, corresponding to a volume of roughly 13 × 160 × 90 mm³. For all further analyses custom MATLAB (R2014a, Mathworks) and R (version 3.2.5, R Development Core Team) scripts were used. A right-handed coordinate system was defined where x and y were, respectively, parallel and perpendicular to the free-stream direction and z parallel to the gravitational axis (figure 1). u , v and w were defined as the velocities in x , y and z directions.

As the moths reacted to the laser light after approximately 2–4 wingbeats (clearly visible in the wake visualisations), only the first, stable wingbeats of each recorded sequence were used in subsequent analyses. In all analyses an average value for all stable wingbeats in a sequence was used as an observation. The start and end frame of a wingbeat was defined by visual inspection of iso-surfaces of vorticity magnitude. To ensure that only stable wingbeats were used, while at the same time allowing for potential weight changes due to feeding during experiments, we excluded wingbeats where weight support was <85% or >115%. In the most extreme individual the weight range during all flights were average ±12%. To avoid

Table 2. Linear fit parameters of the effect of flight speed (u) on stroke plane angle (θ , degrees) and amplitude (A , mm) in the xz plane.

Parameter	Individual	Equation	R^2	Sig.
Stroke plane angle (θ)	M1	$11u + 24$	0.94	***
	M2	$11u + 23$	0.94	***
Stroke plane amplitude (A)	M1	$-7.1u + 76$	0.73	***
	M2	$-5.4u + 79$	0.78	***

losing these data points when setting an acceptable weight support range we had to set the limit to at least $\pm 12\%$, and so it was "rounded up" to $\pm 15\%$. This resulted in 152 wingbeats, or 84 data points.

Kinematics

Simultaneously with the PIV measurements, the kinematics of the flying moths were recorded with two high-speed cameras (HighSpeedStar 3, 1024×1024 pixels, 640 Hz). Four points (front and back of the body, wing base and wing tip) were manually digitised in four wingbeats for each individual and flight speed. The system was calibrated with a checkerboard calibration plate and MATLAB's Computer Vision System Toolbox (mean reprojection error: 0.40–0.45 mm). The triangulated points allowed us to estimate body angle (β) as well as stroke plane angle (θ) and wingbeat amplitude (A). In addition, one frame per individual where the wings were maximally outstretched was used to estimate wing area, wing span and local chord, in 100 steps, along the wing. The measured kinematic and morphological parameters were subsequently used as input in the aerodynamic power models (equations 5-8).

Body angle was only used to graphically determine body drag coefficient ($C_{D,\text{body}}$, for use in equation 6) from [15]. $C_{D,\text{body}}$ ranged between approximately 0.25 and 0.35, but due to the variation in body angles and the non-exact way of determining the corresponding $C_{D,\text{body}}$, we opted to only use an intermediate value (0.3) in subsequent calculations. In the worst case scenario, when the drag from the body is largest relative to the total drag (3.8 ms^{-1} , the other power components at their minimum for this speed), a change in $C_{D,\text{body}}$ of 0.05 causes a 2% change in total power.

Stroke plane data were used for profile drag (P_{pro}) calculations (equation 7), to determine the relative air speed flowing over the different sections along the wing (u_r). We assumed span-wise flow to be a negligible component of (P_{pro}), and thus only measured stroke plane and amplitude in the xz -plane. Both parameters displayed a linear relationship with flight speed (see table 2), and the linearly fitted data were used in the calculations, as this allowed for a continuous equation.

Wingbeat frequency (f) was determined from the PIV data. Regressions showed that while M2 did not linearly vary its frequency with speed ($p = 0.2$, $R^2 = 0.02$), M1 did to some degree ($p = 0.0001$, $R^2 = 0.18$). However, as we preferred to model frequency in a similar way in both individuals, we used the average value over all speeds for each moth in further analysis (see table 1). For M1, this resulted in a predicted power difference never larger than 1.8%, when compared to a model using a linearly increasing frequency.

Measuring Aerodynamic Power and Lift

For each wingbeat we calculated aerodynamic power (P) and lift (L). Since the tomo-PIV generated 3-dimensional vector fields, we could calculate vorticity and velocity gradients directly in each measurement volume, instead of relying on pseudo-volumes, as is required with stereo-PIV data. Lift was then calculated by evaluating the following integral in the centre plane of each volume:

$$L = \rho \left(\iint y u \omega_x dS + \iint y \left(w \frac{\partial u}{\partial y} - v \frac{\partial u}{\partial z} \right) dS \right), \quad (1)$$

where ρ is air density and ω_x is vorticity in the stream-wise direction [22]. This equation is obtained from integrating the Navier-Stokes equations over a control volume surrounding the object of interest in the flow (see *e.g.* [23, 24]), assuming that all but the Trefftz-plane sides have zero perturbations from the free-stream flow. The first term is the most dominant term. A simplified form of this term has frequently been used in animal flight literature for estimating the lift force of a pair of trailing vortices (*e.g.* [25]). The second term in the equation takes into account variation in the stream-wise flow. This term is commonly ignored, assuming a relatively uniform stream-wise flow, but it can be significant at the low flight speeds of animals [22]. Lift was only used for weight support calculations, as a condition for excluding data points from further analysis.

Power was defined as the rate of kinetic energy (E) added to the wake during a wingbeat. As the PIV-volume was thinner than the wavelength of one wingbeat, pseudo-volumes were constructed by stacking the centre plane of each volume in a sequence, and defining $dx = dt \times u_\infty$, where dt is the time between subsequent frames and u_∞ the free-stream velocity. After subtracting u_∞ from the velocity field, to only use the fluctuations in the stream-wise direction, P was calculated (following [18]) as:

$$\begin{aligned} P &= \dot{E} = \frac{1}{2}\rho \iiint (u^2 + v^2 + w^2) (u_\infty + u) dS d\tau \\ &= \frac{1}{2}\rho f \iiint (u^2 + v^2 + w^2) \left(1 + \frac{u}{u_\infty}\right) dV, \end{aligned} \quad (2)$$

where τ is the normalised time during a wingbeat and f is the wingbeat frequency. Equation 2 follows from a derivation similar to that of equation 1, but instead of flow of momentum, it is applied to the flow of energy. The full derivation was described by Drela [18]. The original equation includes a pressure term, but this was found to be negligible when measuring in a Trefftz plane >0.4 wingspans downstream of the wing [18]. As our measurement plane was approximately one wingspan away, the pressure term was omitted.

While vorticity (ω) was confined to our measurement volume, induced airflow was not. As the kinetic energy method depends on finding all velocity added to the air by the animal, we extended the velocity field to the edges of the wind tunnel before evaluating the integral. The extension was performed using a technique similar to [19], which takes advantage of the fact that for an incompressible fluid velocity can be calculated from the stream function (ψ) as

$$\mathbf{u} = \nabla \times \psi \quad (3)$$

The stream function relates to the vorticity field by the Poisson equation:

$$-\omega = \nabla^2 \psi. \quad (4)$$

The spatial domain of the vorticity field was enlarged from approximately $0.1 \times 0.1 \text{ m}^2$ to an area equal to the wind tunnel cross section ($1.05 \times 1.05 \text{ m}^2$); the out-of-view sections were assumed irrotational. To reduce computational cost, we used FFT versions of the equations, with the wake of a full wingbeat periodically repeated. This method requires a volume of one full wingbeat, which was not obtained with our tomo-PIV measurements. Therefore equation 4 was solved using pseudo-volumes of vorticity (calculated from the true 3-dimensional velocity fields). These were constructed by stacking the centre plane of each volume in a sequence, and defining $dx = dt \times u_\infty$, where dt is the time between subsequent frames and u_∞ the free-stream velocity. After obtaining the full velocity field for the whole wind tunnel we replaced, in the central part of the volume, the calculated values with the measured values to increase accuracy. To investigate whether noise in the data was amplified by the method, and thus potentially affecting our results, we also calculated the power from free-stream vorticity fields. These sequences were recorded with the feeder in place, and the measured value is thus a combination of the effects of noise and feeder drag. For all speeds the power was less than 1 % of the average power produced by a moth, and in some cases as little as 0.1 %.

Modelling Aerodynamic Power

In addition to the lift force, which keeps it airborne, a flying animal always produces drag (D). One element of this, the induced drag (D_{ind}), is a direct consequence of producing lift with a finite wing, and scales with the inverse square of the flight speed. The wings and body of the animal will also generate form and friction drag, and these components – the profile drag (D_{pro}) and parasite drag (D_{par}), respectively – scale with the speed squared. To balance the drag, an opposite force, thrust (T) is required. This force requires power (which comes from flapping the wings) to be generated and can simply be calculated as drag multiplied with airspeed. We can therefore predict that the power required to fly is a sum of one component that scales inversely with air speed (induced power, P_{ind}) and two that scales with the cube of the air speed (profile and parasite power, P_{pro} and P_{par}), resulting in the characteristic U-shaped power curve.

While P_{ind} and P_{par} can be rather straightforwardly modelled, calculating P_{pro} of flapping wings is significantly more complex, as the drag on the wings vary throughout the wingbeat and depends on kinematics, wing shape and wing deformations. As a simplification, Pennycuick [2, 3] modelled the profile drag as constant over a small range of cruising speeds, approximately between u_{mp} and u_{mr} , justified by the assumption that the profile drag coefficient ($C_{D,\text{pro}}$) should decrease when flight speed increases. However, this invalidates the model outside of this range of speeds. The blade-element approach instead uses more realistic kinematics, but requires an estimation of $C_{D,\text{pro}}$, which can be very difficult to measure. $C_{D,\text{pro}}$ affects power mainly at high speeds, and an underestimation of this coefficient will result in a slower increase in power with increased flight speeds, and *vice versa*.

Contrarily, the induced power factor (k), a coefficient used to compensate for departure from the ideal case of an elliptic lift distribution and an associated constant downwash along the wing span, mainly affects power at low speeds, with high k resulting in a sharper decrease in power at speeds $< u_{\text{mp}}$. The default value of k in Pennycuick's model for vertebrates is 1.2 [26], but it has recently been estimated to 2.2 in *M. sexta* [21]. We used this range of k -values, together with estimates of $C_{D,\text{pro}}$ from [15] and [27], to form an envelope of possible power curves based on observed kinematics and morphology. In [15], $C_{D,\text{pro}}$ was measured on fixed wings in a wind tunnel. The coefficient was not constant across speeds, but we have here used its average value (over speeds and individuals) for all flight speeds in our model, as the variation was large and did not follow a simple analytical function.

While more complex, and perhaps more realistic, power models have been developed [28], we are here investigating if the classic simple models are a good approximation in insect flight, and are therefore only comparing our data with Pennycuick's model and a slightly modified averaged blade-element model.

To model the power we calculated its three components: induced power (P_{ind}), parasite power (P_{par})

Table 3. Ranges of aerodynamic parameters used in the power models. ρ : air density, k : induced power factor, $C_{D,\text{body}}$: body drag coefficient, $C_{D,\text{pro,d}}$ and $C_{D,\text{pro,u}}$: average profile drag coefficient during downstroke and upstroke, respectively.

Symbol	Range	Source
ρ	1.19	Present study
k	1.2 – 2.2	[26], [21]
$C_{D,\text{body}}$	0.3	[15] and body angle from this study
$C_{D,\text{pro,d}}$	$\left(7/\sqrt{Re}\right) - 0.33$	[27],[15]
$C_{D,\text{pro,u}}$	$\left(7/\sqrt{Re}\right) - 0.14$	[27],[15]

211 and profile power (P_{pro}), as

$$P_{\text{ind}} = kW \sqrt{-\frac{u^2}{2} + \sqrt{\left(\frac{2W}{\rho\pi b^2}\right)^2 + \frac{u^4}{4}}}, \quad (5)$$

212 where u is the air speed, k the induced power factor, W the weight of the moth and b the wingspan.
 213 This equation uses a low-speed correction by Glauert [29] to remove the unreasonable effect that power is
 214 infinitely high at zero flight speed, sometimes present in calculations of P_{ind} .

$$P_{\text{par}} = \frac{1}{2}\rho S_b C_{D,\text{body}} u^3, \quad (6)$$

215 where S_b is the body frontal area and $C_{D,\text{body}}$ the body drag coefficient.

$$P_{\text{pro}} = \frac{1}{2}\rho \sum_{r=0}^R c(r) \frac{u_{r,d}^3 C_{D,\text{pro},d} + u_{r,u}^3 C_{D,\text{pro},u}}{2} \Delta r, \quad (7)$$

216 where r is the radial position ($0-R$) along the wing, $c(r)$ is the local wing chord at r , $C_{D,\text{pro},d}$ and $C_{D,\text{pro},u}$
 217 are the average profile drag coefficients during down- and upstroke, respectively, and $u_{r,d}$ and $u_{r,u}$ are the
 218 average relative air speeds along the moving wing during down- and upstroke.

219 In Pennycuick's [2, 3] vertebrate model, profile power is calculated as

$$P_{\text{pro}} = \frac{8.4 P_{\text{am}}}{AR}, \quad (8)$$

220 where P_{am} is "absolute minimum power", calculated as the sum of P_{ind} and P_{par} at u_{mp} , and AR the
 221 aspect ratio of the wings. The other two power components are identical to the those of the blade-element
 222 model.

223 Both models follow the general speed relationship

$$P = c_1 + c_2 u^{-1} + c_3 u^3. \quad (9)$$

224 We fitted this general form to our measurements of aerodynamic power. We then compared this model
 225 to fitting a straight line. In this way we could evaluate whether a U-shaped curve is a better fit for the
 226 data. The fits were judged based on their R^2 value and the model-choice criteria AICc ("AICc" from the R
 227 package AICcmodavg [30]). This criterion penalises complexity in a model, and the model with the lowest
 228 AICc value is considered to be the best choice. From the best fits, the blade-element model (average of
 229 100×100 steps over k and $C_{D,\text{pro}}$) and Pennycuick's model the characteristic speeds, u_{mp} and u_{mr} , were
 230 calculated.

231 Results

232 Vortex Wake Topology

233 At all speeds measured, the most prominent feature of the vortex wake of *M. sexta* was a pair of strong
 234 tip vortices, sometimes accompanied by much weaker root vortices during the first half of each half-stroke
 235 (figure 2a). The root vortices, spinning in the opposite direction of the same-side tip vortex, reflect a
 236 decrease in lift over the body. Root vortices occurred at speeds from 2 ms^{-1} , occasionally connected by
 237 one or more vortices shed from over the body and aligned in the span-wise direction (figure 2a). While
 238 the wake was superficially similar at all speeds investigated, some speed-dependent patterns could be
 239 discerned upon visual inspection, using iso-surface of constant Q-value [31] (see supplemental figure S1).
 240 First, vortex structures were generally more distinct at higher speeds. At the lowest speed, 1 ms^{-1} , vortices
 241 were so diffused that no closed vortex loops could be observed. Secondly, the upstroke tip vortices seemed

Table 4. R^2 , AICc (Akaike information criterion with a correction for small sample sizes) and significance level for fitting equation 9 (“U-shape”) and a straight line to the power data for each moth. The best fit for each dataset is in bold type.

	R^2 (U-shape)	R^2 (line)	Sig. (U-shape)	Sig. (line)	AICc (U-shape)	AICc (line)
M1	0.29	0.00038	***	n.s.	-399	-385
M2	0.60	0.39	***	***	-326	-313

Table 5. Characteristic speeds u_{mp} and u_{mr} calculated 1) as an average from the envelope of theoretical predictions (range in parentheses), 2) from the fitted curves for the two individuals and 3) from Pennycuick’s flight model for vertebrates, averaged for the two individuals.

	u_{mp} (ms ⁻¹)	u_{mr} (ms ⁻¹)
M1 (fit)	2.2	3.7
M2 (fit)	2.7	4.7
Avg. blade-element model	2.4 (1.9–3.1)	3.6 (3.0–4.4)
Avg. Pennycuick’s model	3.9	6.6

to increase in strength at higher speeds. While the moths at 1 ms⁻¹ (and, occasionally, at 2 ms⁻¹) often appeared to have an aerodynamically almost inactive upstroke, most sequences at 2.8–3.8 ms⁻¹ showed clear tip vortices throughout the whole wingbeat. As can be seen by the wing tip path in figure 3, the upstroke cuts through the air in an arc that is almost vertical at 2.9 ms⁻¹. As the tip vortices during upstroke are of the opposite sense to those of the downstroke, and because of their vertical alignment, they relate to a production of thrust through a backwards directed jet (figure 2c). However, at the end of upstroke the arc has become more horizontal, and the vortex pair induces an upwash, reflecting a downwards-directed force (figure 2b).

As our experiment was conducted using a tomographic PIV system, we were able to capture the three-dimensional properties of the wake vortices. While often imagined as smooth cores of vorticity, the tip vortices instead consisted of several inter-twined vortices. This was most clear at 1 ms⁻¹, but can also be seen in figure 2a. At times, the tip vortex appeared as one larger core entwined by 1–3 smaller vortices, other times as 2–3 similar-sized cores.

Power

Measured power values for the two moths are presented in figure 4. Although the data points show some variation the majority of the values for both individuals lie within the range predicted by the blade-element model. The best fits for the two individuals are shown in figure 4. As can be seen in table 4, the U-shaped curve (equation 9) explains a higher amount of the variation, and has a lower AICc value, than the straight line for both moths, verifying that the power–speed relationship is U-shaped for these individuals.

As can be seen in table 5, the curves fitted to the data and the average blade-element model predicted similar characteristic flight speeds (data fit: u_{mp} =2.2–2.7, u_{mr} =3.7–4.7; model: u_{mp} =2.4, u_{mr} =3.6), while Pennycuick’s model yielded notably higher characteristic speeds (u_{mp} =3.9, u_{mr} =6.6).

Discussion

Vortex Wake Topology

Improved quality of PIV measurements revealed previously undescribed vortex structures. We found multi-cored tip vortices, of which the origin is difficult to determine (but see Henningsson *et al.* [32] for a suggestion). From qualitative analysis of the wake structures we could also infer that the moths produced a downward force during the late upstroke at the higher flight speeds, which contrasts with previous studies [15, 16, 33]. While visualisations of the vertical flow (figure 2b) clearly show an upwash (reflecting

a downward force) at the later stages of the upstroke, previous interpretations of smoke visualisations [16], force calculations [15] and CFD [33] (the latter two based on kinematics data from [34]) have instead come to the opposite conclusion: that lift is being generated. As it is sometimes not possible to judge the sense of rotation from smoke visualisations, it can, in those cases, be difficult to separate the two options.

Our data show that, apart from the obvious function to relocate the wing to the start position of the next downstroke, the main role of the upstroke is to produce thrust at higher flight speed. At 1, and sometimes 2, ms^{-1} , the wake lacks, or has very weak, upstroke vortices, and thrust is therefore mainly generated during downstroke. There is no production of downward force during the upstroke at these speeds. This makes intuitive sense: at higher speeds the drag is higher, so the demand for thrust increases. At the same time it is easier for the animal to produce lift at higher speed, and so the negative weight support produced during the upstroke may not be a problem at these speeds.

When comparing the wake topology to that of other animal groups, it can be noted that a similar pattern to that of *M. sexta* has been found in bats [35]. At speeds above a certain threshold (3 ms^{-1}), the outer part of the bat wing forms a small vortex loop that reflects a downward force during late upstroke. Similar to our study, this is not found at low speeds in bats.

M. sexta has been extensively studied in hovering flight, and in an early paper Weis-Fogh [36] proposed that it performs what the author defines as “normal hovering”, which essentially is equivalent to a symmetrical wingbeat where each half-stroke contributes equally to weight support. The same conclusion was drawn by Casey [37], but a later kinematics study found *M. sexta* to have an asymmetric wingbeat, with, on average, 42% more time spent on the downstroke [34]. In line with Weis-Fogh’s [36] results, several studies [16, 15, 33] have concluded that the upstroke is significantly contributing to weight support in *M. sexta*, in some cases even more than the downstroke [15]. In contrast to these studies, we found no support for an aerodynamically active upstroke at the lowest speeds. While we did not study hovering flight directly, the fact that the upstroke vortices become less strong when flight speed decreases, and are in fact almost absent at near-hovering, suggests that force production during hovering is highly asymmetric between the half-strokes and that weight support is mainly produced during downstroke. This is similar to the asymmetric hovering found in *e.g.* dragonflies and hoverflies [38], as well as hummingbirds [39]. However, we do not exclude the possibility that some information about the wake topology during upstroke may be lost if the wing cuts back through the previously shed wake at very low flight speeds.

Power

Our results show that the classical U-shaped power curve is a reasonable qualitative description of the flight speed–power relationship in, at least, some insect taxa. Comparing this to the multiple J-shaped power curves that have previously been found in other insects, it is interesting that a species that is highly dependent on hovering for its foraging (the proboscis does not extend when the wings are at rest) is the first to show indications of low speeds requiring higher power than intermediate speeds.

In a previous study of hawkmoth flight, *M. sexta* displayed a preference for flight speeds of approximately 3 ms^{-1} when flying freely in a room [21]. Our predictions place this speed between u_{mp} and u_{mr} . The moths in our study were not able to fly at higher speeds than 3.8 ms^{-1} without crashing, and similar behaviour has been shown in previous studies (see *e.g.* [40]). However, we don’t exclude the possibility that individuals in the wild could fly faster, as this is typically the case for wind tunnel studies with free-flying animals. Even though the characteristic flight speeds that were derived from the data corresponds rather well to these two observations, the speeds varied somewhat between the two individuals. This could represent true differences in the flight and morphology of the moths, or be an artefact due to the limited number of data points for, especially, M2 at 3.8 ms^{-1} . The flight speed predictions based on the blade-element model (equations 5–7) were similar to those calculated by the experimental data. However, the range of possible speeds that could be predicted by varying these two parameters showed that the model is quite sensitive to parameter values. Pennycuik’s model (equations 5, 6, 8), which was only used with the default parameter value of $k = 1.2$ ($C_{D,\text{pro}}$ is not explicitly in the model), predicted significantly higher

flight speeds than both the experimental data and the blade-element model. The difference in curve shape and predicted flight speeds between the two models is due to the different scaling of profile power with air speed (blade-element: $P \propto u^{2.5-3}$, Pennycuick: $P \propto 1$), which in turn is caused by different assumptions on how $C_{D,pro}$ is affected by flight speed. In our blade-element model we use the range between a constant $C_{D,pro}$ and one that scales with $u^{-1/2}$ (see table 3), while Pennycuick's model assumes that $C_{D,pro}$ scales with $1/u^3$ and thus fully compensates for the u^3 factor in the P_{pro} equation. Since Pennycuick's approximation of a constant profile power originates from studies on birds, for which this component appears to be relatively constant over cruising speeds [26], it is unsurprising that the blade-element model predicts flight power more accurately for hawkmoths. In addition, Pennycuick's model is only valid between u_{mp} and u_{mr} , a range which starts at the maximum air speed at which our moths were able to fly stably. For these reasons, this model is probably not a good choice for modelling insect flight.

It should be remembered that both models used here, including the $C_{D,pro}$ estimations, are based on quasi-steady-state aerodynamics. How would the presence of a leading edge vortex affect our conclusion that *M. sexta* has a U-shaped power curve? It is likely that a LEV would cause $C_{D,pro}$ to increase, as the vortex creates additional drag on the wing [41]. This would make the U-shape more pronounced. As LEV is a lift-enhancing effect most useful at low speeds [13, 42], one would imagine that $C_{D,pro}$ is higher at low speeds, while close to steady-state values when the flight is faster, resulting in a flatter curve. However, the LEV in *M. sexta* has previously been found to be similar in size at all speeds [11], and even increasing in size with flight speed [16]. Therefore, using unsteady values of $C_{D,pro}$ would probably not change the prediction of a U-shaped power curve with a rather small span of predicted characteristic flight speeds.

Due to experimental restrictions, our moths were feeding at all flight speeds, which may not be completely natural for the species. In the wild, flying at high speeds may require less manoeuvring than during our experiments, which could lead to lower power consumption. This would, in turn, cause the predicted u_{mr} to be slightly higher than our estimations. However, we attempted to minimise this problem by discarding wingbeats that, in the wake visualisations, showed signs of unsteadiness due to manoeuvres. The comparatively high power at near-hover is probably realistic, as the setup more correctly mimics natural conditions in this case.

Energetics

Power is used for several aspects of an animal's flight. In this study we measured specifically the aerodynamic power (P_{aero}) added to the air to keep the study subject airborne. However, power is also needed for acceleration and deceleration of the wings (inertial power, P_{acc}). For this, the flight muscles need to be activated, which uses mechanical power (P_{mech}). Ultimately, all power must come from chemically stored energy, and the rate at which this is depleted is termed metabolic power (P_{met}).

We estimated that our study subjects expend approximately 20 mW of aerodynamic power (P_{aero}) when flying (average of the full dataset). Does this make *M. sexta* an efficient flyer? That question can only be addressed by considering other aspects of the animal's energy budget. A simplified pathway of the energy flow is presented in figure 5, using estimates from previous studies of hovering *M. sexta* to compare with our data for flight at 1 ms^{-1} . From this it can be seen that total flight efficiency (E_{tot}) is approximately 5–6%, assuming previous estimations of P_{met} [43] are reliable. The corresponding value for birds and bats has been estimated to 3–33% [44] and 5.6–15% [45, 19], respectively, making hawkmoth flight relatively inefficient in comparison.

In vertebrates, E_{tot} is usually equated with the mechanical efficiency of the flight muscle ($E_{mech} = P_{mech}/P_{met}$), as P_{acc} is most often considered negligible (see *e.g.* [2]). For insects, however, P_{acc} is a significant portion of the energy budget. In theory, an insect could make its flight more efficient by storing the negative power from the deceleration as elastic energy to use during the next acceleration phase, a mechanism which has both been proposed to be important [46] and of no benefit [47] to hawkmoths. Alternatively, it can be transformed to aerodynamic power or simply dissipate as heat. Dickinson and Lighton [48] proposed a formula for calculating how the negative power should optimally be used, assuming

varying capacity of elastic storage. After estimating P_{aero} and P_{acc} from kinematics and morphology of tethered *Drosophila*, the authors calculated the resulting P_{mech} , which decreased with an increase in storage capacity. Figure 6 shows how the formula instead can be used with estimations of muscle mass-specific P_{mech} , ratio of muscle mass to body mass and P_{acc} available in the literature (as we lack these data for our own specimens) to solve for P_{aero} . The calculated aerodynamic power is then compared to our measured data for 1 ms^{-1} (possibly an underestimation of the hovering power). Here, the aerodynamic power has to decrease when elastic storage capacity is low, since we assume a constant P_{mech} . The predicted lines overlap our measured data only in the cases where muscle ratio = 21%, and thus we can draw the conclusion that it is likely that *M. sexta* has a muscle ratio in the lower end of the range 21-34%. Additionally, in no case within the range of our data does *M. sexta* profit from elastically storing more than 35% of the negative power generated from the deceleration.

Finally, it should be noted that it is not clear whether flight efficiency is constant over flight speeds. Should this not be the case, we cannot expect the flight speeds predicted by the power curve to be used in nature. However, Hedrick *et al.* [40] has recently estimated the response to flight speed in the relative timing of activation of two flight muscles (DLM: dorsolongitudinal and DVM: dorsoventral), something that has previously been shown to affect power input in *M. sexta*. In their study, normalised activation phase of DVM displays a U-shaped response to flight speed, with a minimum value at 2 ms^{-1} . This agrees with the notion that power input and output follow the same pattern, and that the relative effort the animal has to expend can be accurately predicted by aerodynamic theory.

Benefits of Using Tomographic PIV

Calculating aerodynamic power based on measurements of the full 3-dimensional velocity field can be a particularly useful method when studying insects and other slow-flying taxa. While similar to the approach previously taken by [19], the method we have used in this study removes from the power and lift equations the assumption that the free-stream air speed dominates the flow in the x -direction (a uniform flow is however still assumed when stacking the PIV planes). Our improved knowledge about the free-stream flow allows for an added term to the equations; equation 1: $\iint y (w\partial u/\partial y - v\partial u/\partial z) dS$, equation 2: u/u_{∞} .

As can be seen in figure 7, flow fluctuations generated by the animal average almost 30% of the free-stream speed at 1 ms^{-1} . Using this method with only information about the fluctuations in y and z – as is the case with conventional stereo-PIV setups – consequently causes a systematic underestimation of the power required to fly at low speeds, and thus a qualitatively different power curve.

Authors' Contributions

KW and AH conceived and designed the study. KW carried out the experiments and analysis, and drafted the manuscript. MKH and KW implemented the method for measuring aerodynamic power. All authors contributed to the final manuscript.

Acknowledgements

We are grateful to Anna Balkenius at the Swedish University of Agricultural Sciences for providing the moths, to members of the Animal Flight Lab for advice and support, and to two anonymous referees for constructive suggestions that improved the manuscript.

Funding Statement

The tomo-PIV system was funded by an infrastructure grant from Lund University and the research was funded by the Swedish Research Council (grant 621-2012-3585 to A.H. and a Linnaeus grant 359-2007-8690

408 to the Center of Animal Movement Research, CAnMove).

Figures

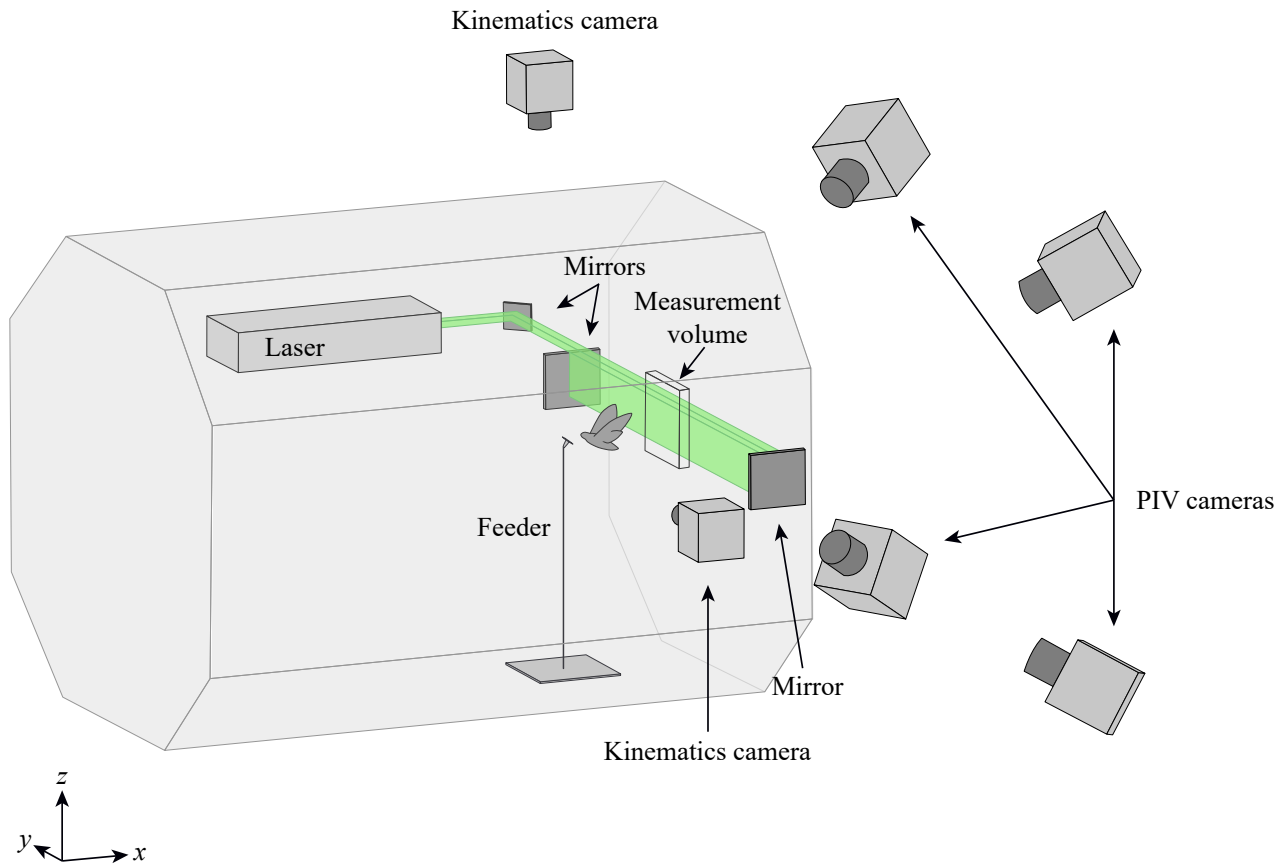


Figure 1. Experimental setup. Test section (1.2 m wide) of the Lund University wind tunnel, with a 14 mm thick measurement volume produced by bouncing laser light between two mirrors. Four PIV-cameras are pointed towards the volume to record particle images, and two kinematics cameras see the free-flying *M. sexta* from the side and above, respectively. The feeder is placed 190 mm from the laser sheet.

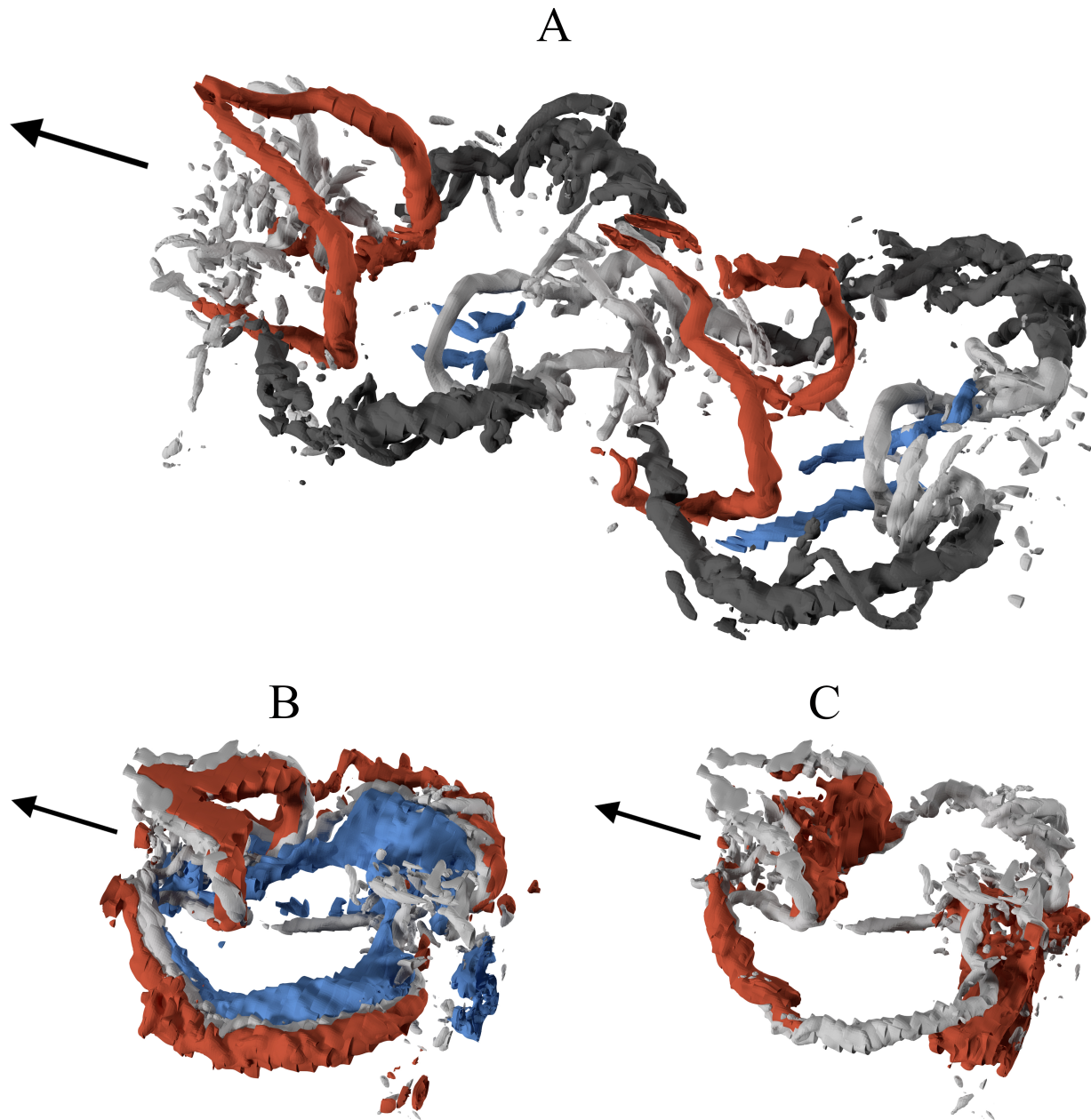


Figure 2. Wake visualisations of M1 flying at 2.9 ms^{-1} . Arrows indicate flight direction. (A) shows iso-surface of constant Q-value ($Q=70000$). Multi-cored downstroke tip vortices are shown in dark grey, downstroke root vortex in blue and upstroke tip vortices in red. Vorticity released over the body can be seen in light grey crossing the root vortices. (B) and (C) show iso-surface of constant Q-value ($Q=85000$) in grey. In (B), downwards-directed velocities are shown in blue ($V=-1.5 \text{ ms}^{-1}$) and upwards-directed in red ($V=0.8 \text{ ms}^{-1}$), reflecting lift and a downwards force, respectively. (C) shows thrust-generating velocities ($U=4 \text{ ms}^{-1}$, including the free-stream speed) in red.

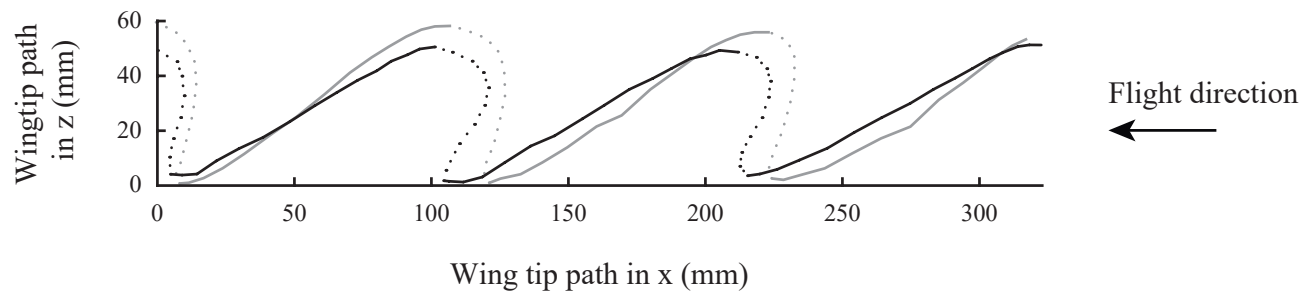


Figure 3. Side view of the wing tip path of M1 (black) and M2 (grey) flying at 2.9 ms^{-1} . Downstroke as solid line, upstroke as dotted.

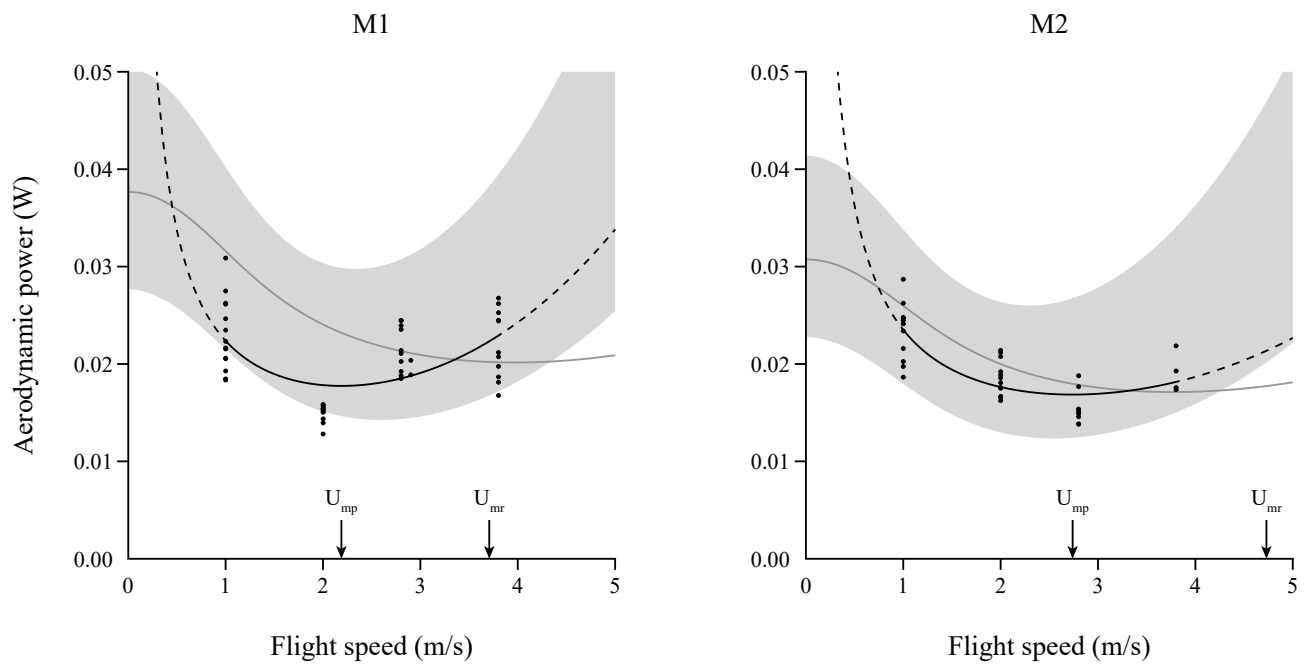


Figure 4. Aerodynamic power of M1 and M2 flying at $1\text{--}3.8 \text{ ms}^{-1}$. Measured power shown as filled circles, with the best fit (equation 9) for each individual as a black curve. Dashed line indicates an extrapolation outside of our measurement range. Blade-element model (equations 5–7) as a grey band, Pennycuick's model (equations 5–6, 8) as grey curve, both using model parameters from tables 1–3.

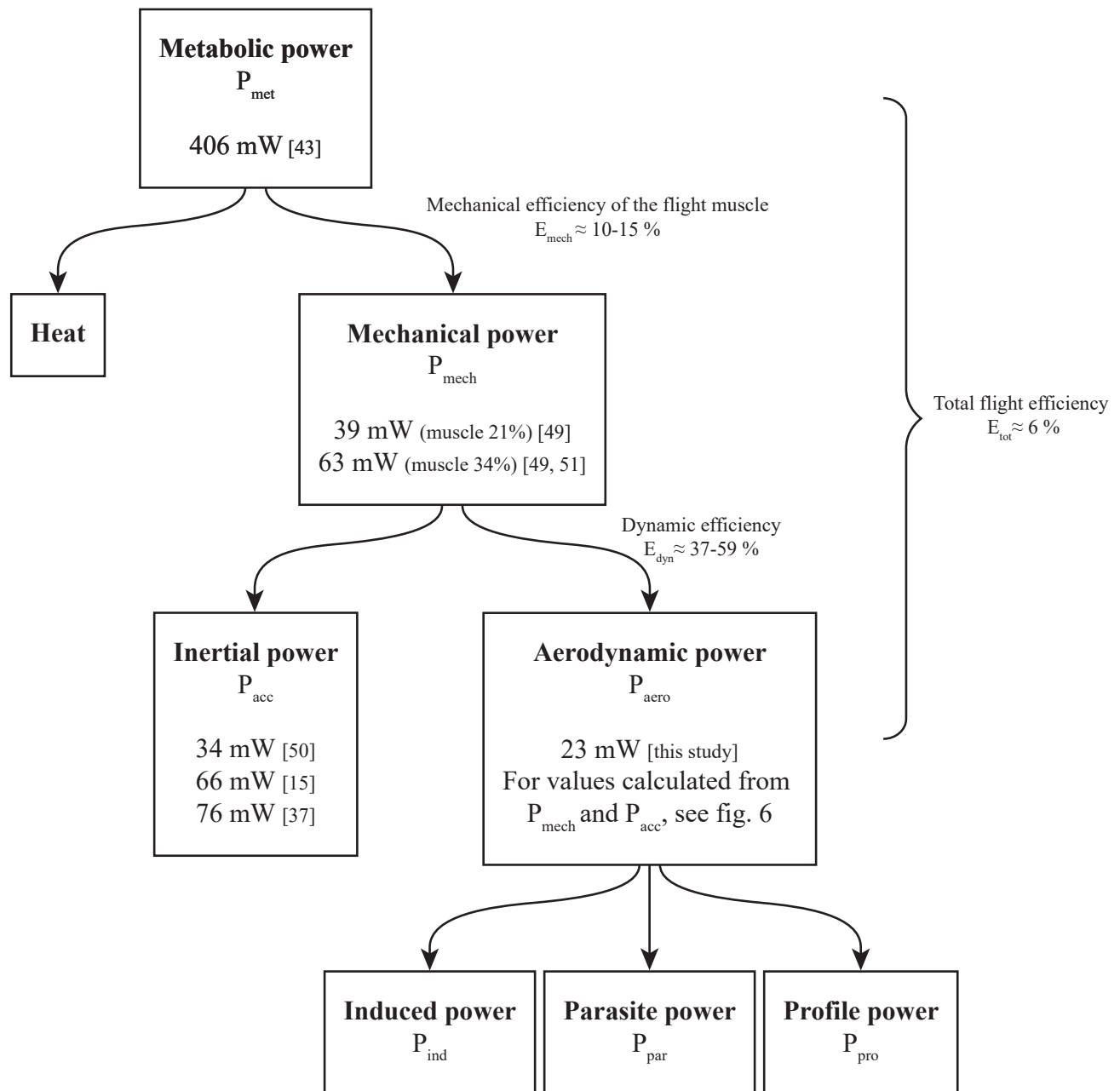


Figure 5. Pathway of energy expenditure in a flying *M. sexta* with a body mass of 2.1 g (the average mass of our two individuals), modified after [37]. Includes estimates of power components from hovering *M. sexta* [15, 37, 43, 49, 50]. Estimates for flight muscle ratio from [49] (*M. sexta*) and [51] (*Manduca sp.*). The value from this study is for flight at 1 ms^{-1} .

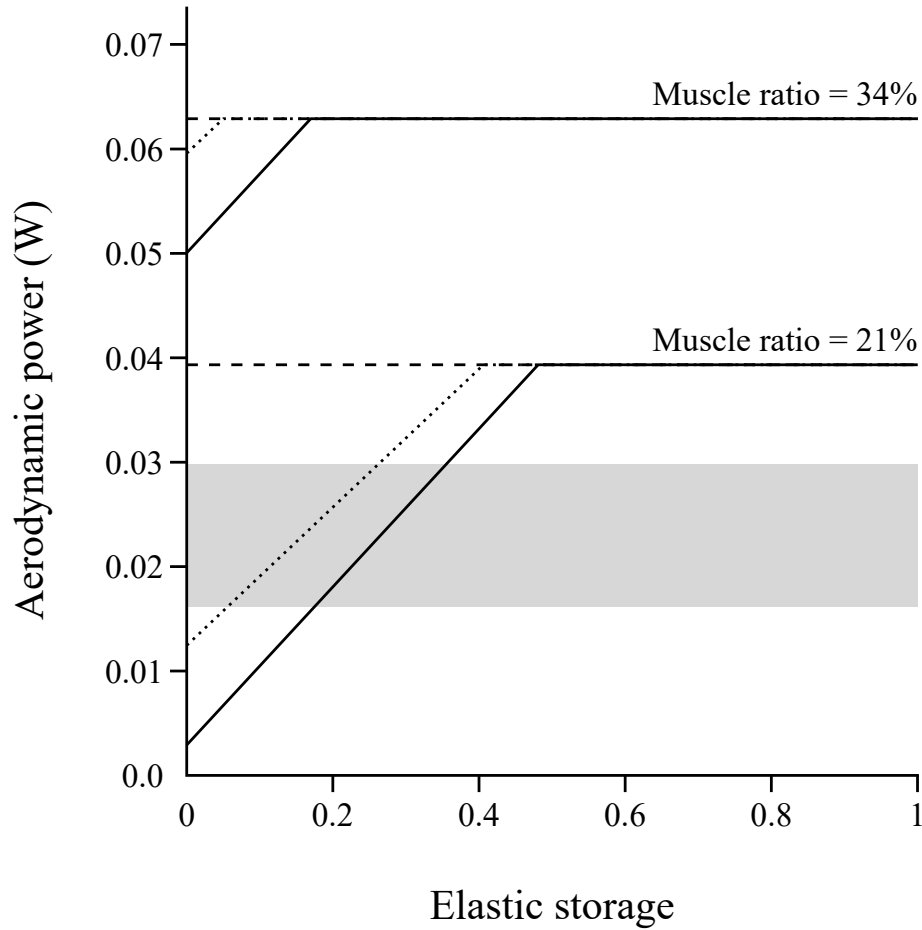


Figure 6. P_{aero} during hovering predicted from P_{mech} assuming different P_{acc} from the literature (dashed lines: $P_{acc} = 16.4 \text{ Wkg}^{-1}$, [50]; dotted lines: $P_{acc} = 31.8 \text{ Wkg}^{-1}$, [15]; solid lines: $P_{acc} = 36.4 \text{ Wkg}^{-1}$, [37]). P_{mech} was calculated as the product of the muscle mass-specific mechanical power ($P_{mech,spec,muscle} = 90 \text{ Wkg}^{-1}$, [49]), the ratio of muscle mass to body mass, estimated to two different values ($m_{muscle}/m = 21\%$, [49]; $m_{muscle}/m = 34\%$, [51]) and average body mass of our two moths ($m = 2.1 \text{ g}$). Equations from [48] were used for the calculations, solving for P_{aero} . For comparison, the grey band shows the total aerodynamic power at 1 ms^{-1} from this study (mean ± 2 standard deviations). All values were measured or calculated for hovering *M. sexta*, except [51], which used an unspecified *Manduca* species.

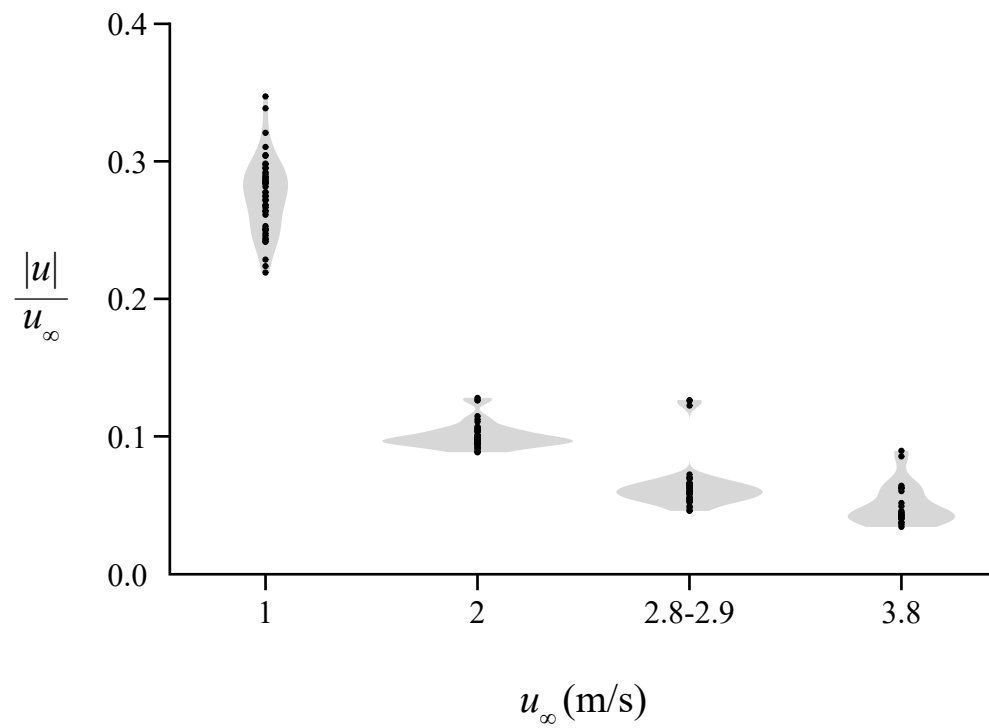


Figure 7. Fluctuations in stream-wise direction ($|u|/u_\infty$) at different flight speeds (u_∞). Filled circles represent wingbeats for both individuals, shaded area kernel density estimation of the data.

Supplemental figure

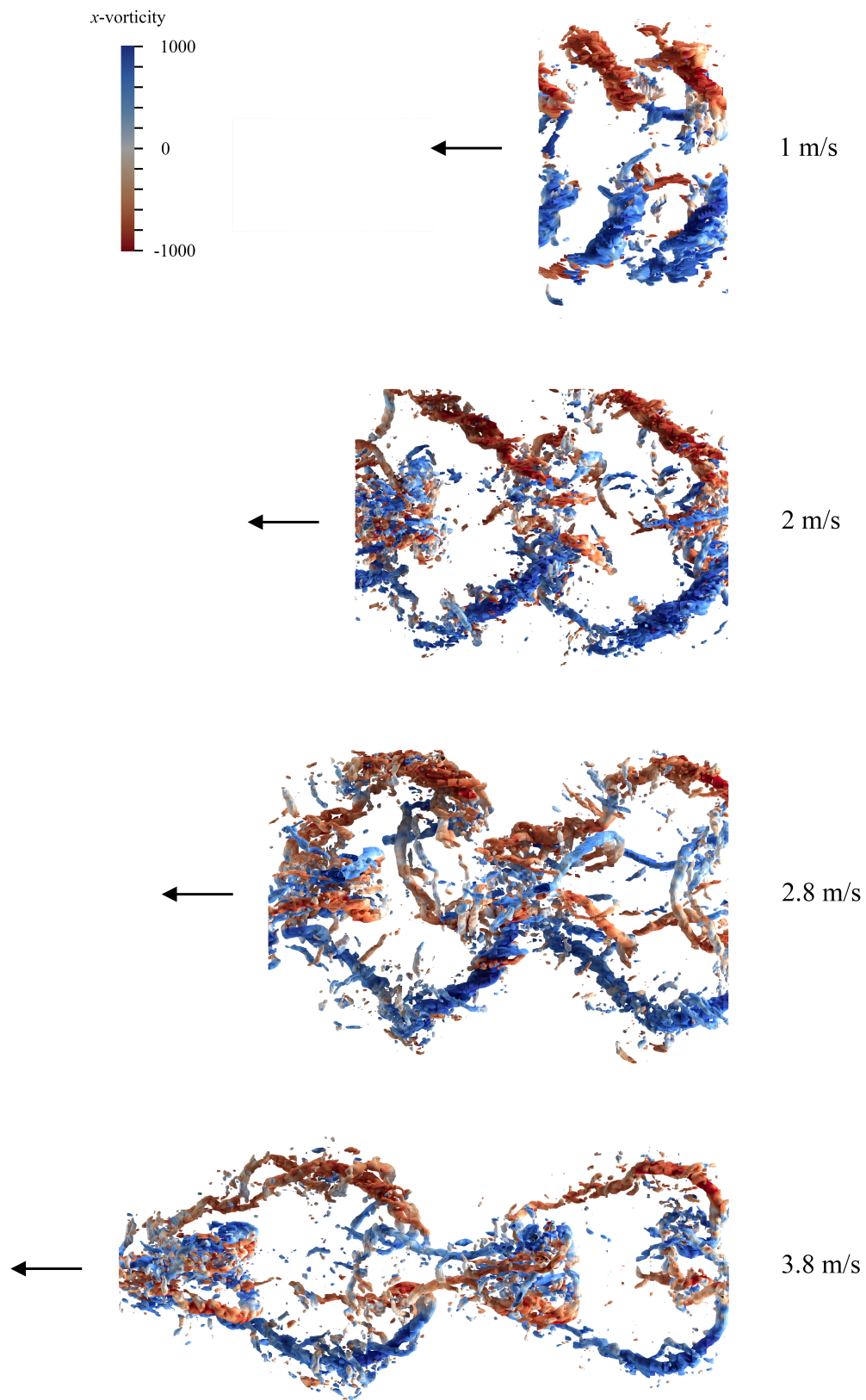


Figure S1. Wake visualisations of M2 flying at 1 and 3.8 ms^{-1} and M1 flying at 2 and 2.8 ms^{-1} . Arrows indicate flight direction. The figure shows iso-surfaces of constant Q -value ($Q=150000$ at 1 and 2 ms^{-1} , 120000 at 2.8 ms^{-1} and 100000 at 3.8 ms^{-1}). The wakes are coloured by vorticity in x -direction.

References

1. Hedenström A, Ålerstam T, 1996 Skylark optimal flight speeds for flying nowhere and somewhere. *Behav. Ecol.* **7**, 121–126. doi:10.1093/beheco/7.2.121.
2. Pennycuik CJ, 2008 *Modelling the Flying Bird*. Oxford, UK: Elsevier.
3. Pennycuik CJ, 1968 Power requirements for horizontal flight in the pigeon *Columba livia*. *J. Exp. Biol.* **49**, 527–555.
4. Hedenström A, Ålerstam T, 1995 Optimal Flight Speed of Birds. *Phil. Trans. R. Soc. Lond. B* **348**, 471–487.
5. Tobalske BW, Hedrick TL, Dial KP, Biewener AA, 2003 Comparative power curves in bird flight. *Nature* **421**, 363–366. doi:10.1038/nature01284.
6. Engel S, Bowlin MS, Hedenström A, 2010 The Role of Wind-Tunnel Studies in Integrative Research on Migration Biology. *Integr. Comp. Biol.* **50**, 323–335. doi:10.1093/icb/icq063.
7. Srygley RB, 2001 Sexual differences in tailwind drift compensation in *Phoebis sennae* butterflies (Lepidoptera: Pieridae) migrating over seas. *Behav. Ecol.* **12**, 607–611. doi:10.1093/beheco/12.5.607.
8. Ellington CP, Machin KE, Casey TM, 1990 Oxygen consumption of bumblebees in forward flight. *Nature* **347**, 472–473. doi:10.1038/347472a0.
9. Sun M, Wu JH, 2003 Aerodynamic force generation and power requirements in forward flight in a fruit fly with modeled wing motion. *J. Exp. Biol.* **206**, 3065–3083. doi:10.1242/jeb.00517.
10. Wu J, Sun M, 2005 Unsteady aerodynamic forces and power requirements of a bumblebee in forward flight. *Acta Mech. Sinica* **21**, 207–217. doi:10.1007/s10409-005-0039-5.
11. Bomphrey RJ, Lawson NJ, Harding NJ, Taylor GK, Thomas ALR, 2005 The aerodynamics of *Manduca sexta*: digital particle image velocimetry analysis of the leading-edge vortex. *J. Exp. Biol.* **208**, 1079–1094. doi:10.1242/jeb.01471.
12. Johansson LC, Engel S, Kelber A, Heerenbrink MK, Hedenström A, 2013 Multiple leading edge vortices of unexpected strength in freely flying hawkmoth. *Sci. Rep.* **3**. doi:10.1038/srep03264.
13. Dudley R, Ellington CP, 1990 Mechanics of Forward Flight in Bumblebees: II. Quasi-steady Lift and Power Requirements. *J. Exp. Biol.* **148**, 53–88.
14. Wakeling JM, Ellington CP, 1997 Dragonfly flight. III. Lift and power requirements. *J. Exp. Biol.* **200**, 583–600.
15. Willmott AP, Ellington CP, 1997 The mechanics of flight in the hawkmoth *Manduca sexta*. II. Aerodynamic consequences of kinematic and morphological variation. *J. Exp. Biol.* **200**, 2723–2745.
16. Willmott AP, Ellington CP, Thomas ALR, 1997 Flow visualization and unsteady aerodynamics in the flight of the hawkmoth, *Manduca sexta*. *Phil. Trans. R. Soc. Lond. B* **352**, 303–316. doi:10.1098/rstb.1997.0022.
17. Bomphrey R, Lawson N, Taylor G, Thomas A, 2006 Application of digital particle image velocimetry to insect aerodynamics: measurement of the leading-edge vortex and near wake of a Hawkmoth. *Exp. Fluids* **40**, 546–554. doi:10.1007/s00348-005-0094-5.
18. Drela M, 2009 AIAA 09-3762 Power balance in aerodynamic flows. In *27th AIAA Applied Aerodynamics Conference June 22 – 25*. San Antonio, TX.

19. von Busse R, Waldman RM, Swartz SM, Voigt CC, Breuer KS, 2014 The aerodynamic cost of flight in the short-tailed fruit bat (*Carollia perspicillata*): comparing theory with measurement. *J. R. Soc. Interface* **11**, 20140147–20140147. doi:10.1098/rsif.2014.0147.
20. Pennycuik C, Alerstam T, Hedenström AH, 1997 A new low-turbulence wind tunnel for bird flight experiments at Lund University, Sweden. *J. Exp. Biol.* **200**, 1441–1449.
21. Henningsson P, Bomphrey RJ, 2013 Span efficiency in hawkmoths. *J. R. Soc. Interface* **10**, 20130099. doi:10.1098/rsif.2013.0099.
22. van Dam CP, Nikfetrat K, Vijgen PMHW, 1993 Lift and drag calculations for wings and tails: Techniques and applications. In AY Cheer, CP Van Dam, editors, *Fluid Dynamics in Biology*, 463–472. American Mathematical Society.
23. Noca F, 1997 *On the evaluation of time-dependent fluid-dynamics forces on bluff bodies*. Ph.D. thesis.
24. Oudheusden BWv, Scarano F, Roosenboom EWM, Casimiri EWF, Souverein LJ, 2007 Evaluation of integral forces and pressure fields from planar velocimetry data for incompressible and compressible flows. *Exp. Fluids* **43**, 153–162. doi:10.1007/s00348-007-0261-y.
25. Henningsson P, Muijres FT, Hedenström A, 2011 Time-resolved vortex wake of a common swift flying over a range of flight speeds. *J. R. Soc. Interface* **8**, 807–816. doi:10.1098/rsif.2010.0533.
26. Pennycuik CJ, 1975 Mechanics of Flight. In DS Farner, JR King, editors, *Avian Biology: Volume V*. New York: Academic Press.
27. Ellington CP, 1984 The Aerodynamics of Hovering Insect Flight. VI. Lift and Power Requirements. *Phil. Trans. R. Soc. Lond. B* **305**, 145–181. doi:10.1098/rstb.1984.0054.
28. Klein Heerenbrink M, Johansson LC, Hedenström A, 2015 Power of the wingbeat: modelling the effects of flapping wings in vertebrate flight. *Proc. R. Soc. Lond. A* **471**, 20140952. doi:10.1098/rspa.2014.0952.
29. Glauert H, 1926 A general theory of the autogyro. *Reports and Memoranda 1111, British ARC* .
30. Mazerolle MJ, 2016 *AICcmodavg: Model selection and multimodel inference based on (Q)AIC(c)*. R package version 2.1-0.
31. Kolář V, 2007 Vortex identification: New requirements and limitations. *Int. J. Heat Fluid Fl.* **28**, 638–652. doi:10.1016/j.ijheatfluidflow.2007.03.004.
32. Henningsson P, Michaelis D, Nakata T, Schanz D, Geisler R, Schröder A, Bomphrey RJ, 2015 The complex aerodynamic footprint of desert locusts revealed by large-volume tomographic particle image velocimetry. *J. R. Soc. Interface* **12**, 20150119. doi:10.1098/rsif.2015.0119.
33. Liu H, Ellington CP, Kawachi K, Berg Cvd, Willmott AP, 1998 A computational fluid dynamic study of hawkmoth hovering. *J. Exp. Biol.* **201**, 461–477.
34. Willmott AP, Ellington CP, 1997 The mechanics of flight in the hawkmoth *Manduca sexta*. I. Kinematics of hovering and forward flight. *J. Exp. Biol.* **200**, 2705–2722.
35. Hedenström A, Johansson LC, Wolf M, Von Busse R, Winter Y, Spedding GR, 2007 Bat flight generates complex aerodynamic tracks. *Science* **316**, 894–897. doi:10.1126/science.1142281.
36. Weis-Fogh T, 1973 Quick Estimates of Flight Fitness in Hovering Animals, Including Novel Mechanisms for Lift Production. *J. Exp. Biol.* **59**, 169–230.

37. Casey TM, 1981 A Comparison of Mechanical and Energetic Estimates of Flight Cost for Hovering Sphinx Moths. *J. Exp. Biol.* **91**, 117–129.
38. Wang ZJ, 2005 Dissecting insect flight. *Annu. Rev. Fluid Mech.* **37**, 183–210. doi:10.1146/annurev.fluid.36.050802.121940.
39. Warrick DR, Tobalske BW, Powers DR, 2005 Aerodynamics of the hovering hummingbird. *Nature* **435**, 1094–1097. doi:10.1038/nature03647.
40. Hedrick TL, Martínez-Blat J, Goodman MJ, 2017 Flight motor modulation with speed in the hawk-moth *Manduca sexta*. *J. Insect Physiol.* **96**, 115–121. doi:10.1016/j.jinsphys.2016.10.003.
41. Polhamus EC, 1966 A concept of the vortex lift of sharp-edge delta wings based on a leading-edge-suction analogy. *NASA Technical Note* **D-3767**.
42. Ellington CP, 1984 The Aerodynamics of Hovering Insect Flight. IV. Aerodynamic Mechanisms. *Phil. Trans. R. Soc. Lond. B* **305**, 79–113. doi:10.2307/2396075.
43. Casey TM, 1976 Flight energetics of sphinx moths: power input during hovering flight. *J. Exp. Biol.* **64**, 529–543.
44. Videler JJ, 2005 *Avian flight*. Oxford: Oxford University Press.
45. Norberg UM, Kunz TH, Steffensen JF, Winter Y, von Helversen O, 1993 The cost of hovering and forward flight in a nectar-feeding bat, *Glossophaga soricina*, estimated from aerodynamic theory. *J. Exp. Biol.* **182**, 207–227.
46. Dudley R, 2000 *The Biomechanics of Insect Flight*. Princeton: Princeton University Press.
47. Sun M, Du G, 2003 Lift and power requirements of hovering insect flight. *Acta Mech. Sinica* **19**, 458–469. doi:10.1007/BF02484580.
48. Dickinson M, Lighton J, 1995 Muscle Efficiency and Elastic Storage in the Flight Motor of *Drosophila*. *Science* **268**, 87–90. doi:10.1126/science.7701346.
49. Stevenson RD, Josephson RK, 1990 Effects of Operating Frequency and Temperature on Mechanical Power Output from Moth Flight Muscle. *J. Exp. Biol.* **149**, 61–78.
50. Zhao L, Deng X, 2009 Power distribution in the hovering flight of the hawk moth *Manduca sexta*. *Bioinspiration & Biomimetics* **4**, 046003. doi:10.1088/1748-3182/4/4/046003.
51. Marden JH, 1987 Maximum Lift Production During Takeoff in Flying Animals. *J. Exp. Biol.* **130**, 235–258.